Materials Science & Engineering C 110 (2020) 110724

Contents lists available at ScienceDirect

Materials Science & Engineering C

journal homepage: www.elsevier.com/locate/msec

Dopamine functionalized CuO nanoparticles: A high valued "turn on" colorimetric biosensor for detecting cysteine in human serum and urine samples

Deepak Rohilla[a], Savita Chaudhary[a,*], Navneet Kaur[b], Asifkhan Shanavas[b]

[a] Department of Chemistry and Centre of Advanced Studies in Chemistry, Panjab University, Chandigarh 160014, India
[b] Institute of Nano Science and Technology (INST), Mohali, Punjab, India

ARTICLE INFO

Keywords:
Copper oxide
Dopamine
L-cysteine
Microwave synthesis
DFT analysis

ABSTRACT

An attempt has been made to design one step synthesis of dopamine coated copper oxide nanoparticles (CuO@DOP NPs) by using microwave radiation method. The luminescent properties of CuO@DOP NPs have been explored for making colorimetric and visual biosensor for L-cys. Natural occurring dopamine has used as a precursor for the coating of CuO NPs that provides stability and generates functionality for the sensing of L-Cysteine (L-Cys). Being one of the important amino acid, L-cys has shown a fundamental role in living species due to the existence of sulfhydryl bonding which further affect the process of protein synthesis in living system. Therefore sensing of L-cys by using CuO@DOP NPs deserves higher consideration. Further, morphological and size parameters have been analyzed by using FESEM and HRTEM techniques. Surface interaction and coating of dopamine over CuO NPs has been examined through FTIR and TGA analysis. The non-toxicity and bio-compatibility of CuO@DOP NPs has been evaluated against L929 cell lines and on bacterial species. A computational study using DFT has been performed to check the possible mechanism of interaction between the CuO@DOP NPs and L-Cys. The higher value of detection limit (35 nM) has further shown its potential scope in sensing L-cys. The interference studies in presence of other amino acids have also taken into consideration for checking the selectivity and sensitivity of designed sensor. The applicability of prepared sensor has further been tested for real human blood serum and urine samples for detecting the presence of L-Cys. The as developed sensor of CuO@DOP NPs has provided rapid and selective sensing ability towards L-Cys over a wide range of concentration and bio-compatibility towards living entity.

Novelty statement: Herein, the application of unique chemical and photo-luminescent properties of CuO NPs have been chosen for the fabrication of new type of fluorophore to complement conventional types of biosensor for L-Cys. The synthesis of CuO based biosensor has been achieved via an economically viable microwave assisted method. The article has not been published in any language anywhere and that it is not under simultaneous consideration by another journal. The current work is novel.

1. Introduction

Out of diverse range of available amino acids, L-Cysteine (L-Cys) is considered as one of the semi-essential type of amino acids with intracellular concentration varies between 20 and 200 μM in the biological system [1–3]. L-Cys plays a significant role in maintaining different types of cellular changes in the living systems and the existence of sulfhydryl bonding in L-Cys has further supported the protein synthesis in living system [4]. In addition, the antioxidative properties of L-Cys have promoted the detoxification rate, balanced blood sugar level, and have supported the proper digestive functioning in living beings [5–7]. Therefore any kind of disruption and deficiencies of L-Cys are related with the problems of liver and skin [8]. The non-regulated L-Cys levels are also associated with the existence of diseases like Alzheimer's, neurotoxicity and abnormal hematopoiesis [9,10]. In addition, the deficiency of L-Cys has caused disabled antioxidative defence with reduced metabolic rate, retarded growth among small children, weak immunity and cancer in extreme cases [11–13]. Hence, the quantification of L-Cys is exceptionally vital from biological and pharmacological point of view [14].

Till now, different types of procedural methods such as high-performance liquid chromatography (HPLC) [15], gas chromatography,

* Corresponding author.
E-mail address: schaudhary@pu.ac.in (S. Chaudhary).

https://doi.org/10.1016/j.msec.2020.110724
Received 21 October 2019; Received in revised form 14 January 2020; Accepted 3 February 2020
Available online 04 February 2020
0928-4931/

mass spectrometry [16,17], and electrochemical sensing [18–20] have been used for the schematic quantification of L-Cys. Yet, majority of the pioneering methods have required skilled personal and costly instrumental facilities [21]. The complicated sample preparation procedures have further constrained their viable utilities [22]. Therefore, the application of nanotechnology plays a potential role to solve these associated problems because of their incredible surface area, magnetic [23] and optical properties. Researchers have significantly achieved degradation/removal of organic pollutants [24–26], detection of metal ions [27–31] and drug concentration [32] via using the surface modification of nanoparticles. Sensing techniques like potentiometry [33–36], ion selective electrode [37–39], voltammetric sensors [40,41] and SERS based biosensors [42,43] have upgraded the previous procedural methodology in the estimation of L-cys, but still there is a lot of scope in on-site detection [46,44]. Contrarily, the colorimetric sensing [45–47] technique has displayed gratifying potential towards the selective and sensitive detection of L-Cys. The fast reaction time and simple working process of colorimetric sensors have overcome the restrictions of pioneer sensing methodologies [48]. Recently, several types of fluorescent chemosensor [49,50] have been developed for the quantification of L-Cys [51,52]. For instance Manna et al. [53] have used the application of benzothiazole–quinoline based conjugates for the selective detection of L-Cys. The interaction of the chosen probe has the tendency to undergo Michael addition reaction while interacting with L-Cys and produced the thio-ether complex. Yang et al. [54] have used the cleavage reaction for producing the white light emitting strategy for the detection of L-Cys. The developed system has wide range of applicability with pH variation from 7 to 12. Wang et al. [55] have prepared the coumarin–salicylaldehyde hydrazone fluorescent ligand for the detection of L-Cys in presence of diverse range of thiols and other amino acids. Further Zhang et al. and Ge et al. have designed label free [56,57] methodology for the detection of biothiols including cysteine, glutathione and homocysteine [58]. Recently, a colorimetric dual signal probe, 1((E)-2-(2-(4-formylstyryl)-4H-chrome4ylidene) malononitrile) has been developed by using complex organic reaction by Huang et al. for the selective sensing of L-Cys from human serum samples [59]. Still, the fabrication of turn-on and off-on-off colorimetric and visual biosensor for L-Cys [60–62] with superior sensitivity and selectivity in presence of interfering amino acids is quite challenging and required sincere efforts from scientific community.

Herein, the application of unique chemical and photo-luminescent properties of CuO NPs have been chosen for the fabrication of new type of fluorophore to complement conventional types of biosensor for L-Cys. CuO NPs and their composites have possessed unique electrical, chemical and thermal stability with large availability of active surface area for better sensing or detection ability [63,64]. The synthesis of CuO based biosensor has been achieved via an economically viable microwave assisted method and enhanced the scope of the methodology in sensing (Fig. 1). The surface modification of the nanoparticles has been done by using DOP [65]. The toxicity analysis of DOP capped CuO NPs (CuO@DOP) have been done against L929 cell by employing MTT assay. The respective geometrical optimizations, energy calculations and chemical interaction between the surface modifier and L-Cys moieties have been properly described by using density functional theory (DFT). The as prepared biosensor has provided a scaffold potential in sensing and novelty due to the following characteristic features: (i) the surface modification of the CuO with DOP has presented a better size control during the single step synthesis (ii) the surface modification has produced better control over the surface area, optical and luminescence properties of CuO nanoparticles and enhanced the catalytic sites on CuO, which are quite beneficial to ameliorate their biosensing activity. In addition, the fast response of CuO@DOP NPs and admirable selectivity has enabled the sequential detection of L-Cys in human serum and urine samples. The detailed UV–vis. and fluorescence measurements have provided deep insight into the mechanistic aspect of L-Cys sensing. The significant aspect of CuO@DOP NPs has been associated with its biocompatibility and lower detection limit which will further assisted their pre-clinical applications and made it a potential contender in bio-sensing applications.

2. Experimental section

2.1. Chemicals

Copper chloride ($CuCl_2$), **2-(3,4-Dihydroxyphenyl)ethylamine hydrochloride** (Dopamine hydrochloride, DOP), L-valine (Val), L-arginine (Arg), L-aspartic acid (Asp), L-glycine (Gly), L- cysteine (Cys), L-histidine (His), L-isoleucine (Ile), L-alanine (Ala), L-leucine (Leu), L-lysine (Lys), L-methionine (Met), L-serine (Ser), L-tyrosine (Tyr), L-tryptophan (Trp), and threonine (Thr) were procured from Sigma Aldrich with purity > 99%. The nitrate salts of Na^+, K^+, NH_4^+, Ni^{2+}, Ba^{2+}, Zn^{2+}, Pb^{2+}, Ca^{2+}, Mg^{2+}, Mn^{2+}, Fe^{2+}, Yb^{3+}, Gd^{3+}, Pr^{3+}, and Ce^{3+} were procured from Avra India with purity > 98%. Doubly distilled water was utilized throughout for the sample preparation.

2.2. Instrumentation

The microwave radiation source with power 800 W and 2450 MHz frequency was used for fabrication of CuO@DOP NPs. X-ray diffraction (XRD), Panalytical, D/Max-2500 was utilized for examining the crystalline phase of CuO@DOP NPs in the 2θ range of 10–90°, while the morphological characterization of CuO@DOP NPs was carried out on transmission electron microscope (TEM), H-7500 from Hitachi at 100 kV. The surface of the CuO@DOP NPs was scrutinized by using a scanning electron microscope (SEM), Hitachi (SU8010), while the mode of interaction between DOP and CuO nanoparticles was checked by

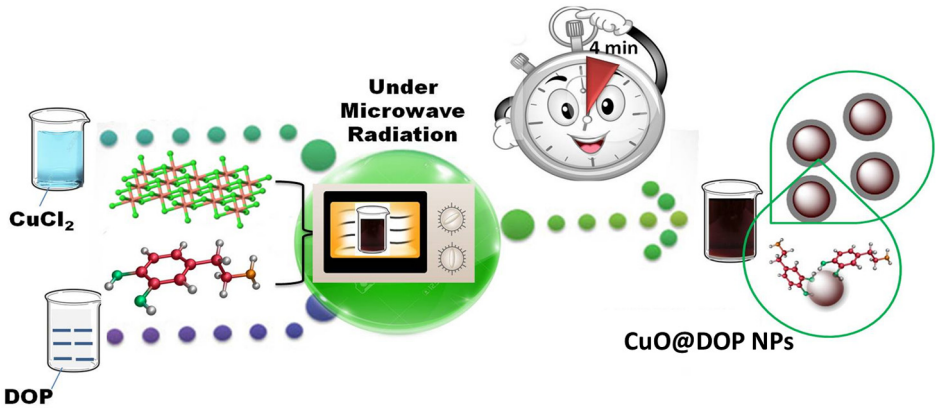

Fig. 1. Schematic illustration showing the microwave-assisted synthesis of CuO@DOP NPs.

using Perkin-Elmer (RX1) FTIR spectrometer in the frequency range of 4400–400 cm^{-1}. The optical absorption and fluorescence emission studies were done on Jasco V550 UV–vis spectrometer and Perkin-Elmer LS 55 fluorescence spectrophotometer respectively. Nano S 90 (Red badge) Malvern Instruments Corporation model no. ZEN 1690 was used for the determination of particle size estimation. The zeta potential measurements were done on the Zetasizer Nano ZSP Malvern Instruments Corporation, UK.

2.3. Microwave assisted synthesis and toxicity profiling of CuO@DOP NPs

2.3.1. Synthesis of CuO@DOP NPs

The surface functionalized CuO NPs were produced by employing the microwave assisted methodology. The chosen methodology considered as the quite simple, economical and fast for making the one pot synthesis of CuO@DOP NPs. The current method found to be more viable and simplified the synthetic procedure to one-pot and overcome the limitations of traditionally employed methods [66]. In brief, the concentration ranging from 1.5 mM to 5 mM of $CuCl_2$ was mixed with 0.6 mM solution of dopamine hydrochloride in aqueous media. The resultant mixture was placed inside the microwave radiation chamber over a frequency range of 2500 MHz for 4 min. The obtained dark wine coloration confirmed the formation of CuO@DOP NPs (Fig. 1). The formed particles were thoroughly washed with the help of centrifugation at 12,000 rpm for 12 min by using water and ethanol and further dried for subsequent analysis.

2.3.2. Toxicity profiling of CuO@DOP NPs

The environmental fate of the prepared nanoparticles was tested by analyzing their in-vitro biocompatibility studies as a function of concentration of nanoparticles. In brief, MTT assay against L929 cell lines was employed for testing the in vitro biocompatibility of CuO@DOP NPs [67]. For the analysis, 0.2 ml of L929 cells was placed in a culture plate for 1 day at 310 K under the atmosphere of 5% CO_2. The cytotoxic effect of CuO@DOP NPs was analyzed as a function of concentration to the L929 cells. All the analysis was done in triplicate. The chosen cells of L929 were washed three times with pre-heated 1× PBS for eliminating the traces of the sample. After 4 h of incubation, the respective measurements of 0.02 ml MTT solutions (5 mg/ml in PBS) were done by diluting the sample with 0.18 ml solution of media. After 240 min, the respective plates were centrifuged with a speed of 1500 rpm for 300 s at room temperature. In order to solubilise the formazan crystals, around 0.150 ml DMSO was appended to each well and noted down the respective absorbance values. ELISA reader was employed for measuring the absorbance value of the suspension at 595 nm. The viability rate of L929 cells were further calculated for detecting the biocompatibility rate of nanoparticles [68]. The antimicrobial activities of CuO@DOP NPs were examined on *Staphylococcus aureus* (gram positive) and *Escherichia coli* (gram negative) strains. For the analysis, 0.08 ml of bacterial strains was transferred on the prepared surface of MH agar in sterilized petri plates. All the prepared plates were cultivated at 308 K for one night to form the zone of inhibitions in presence of different concentrations of CuO@DOP NPs. The value of effective zone of inhibition was estimated by deducting the zone of inhibition for control system.

2.4. Selective sensing of L-Cys and computational studies

Fifteen types of amino acid i.e. L-valine (Val), L-arginine (Arg), L-aspartic acid (Asp), L-glycine (Gly), L-cysteine (L-Cys), L-histidine (His), L-isoleucine (Ile), L-alanine (Ala), L-leucine (Leu), L-lysine (Lys), L-methionine (Met), L-serine (Ser), L-tyrosine (Tyr), L-tryptophan (Trp), and threonine (Thr) were used to test the selectivity of CuO@DOP NPs against amino acids. The selective sensing of L-Cys was further tested in presence of nitrate salts of Na^+, K^+, NH_4^+, Ni^{2+}, Ba^{2+}, Zn^{2+}, Pb^{2+}, Ca^{2+}, Mg^{2+}, Mn^{2+}, Fe^{2+}, Yb^{3+}, Gd^{3+}, Pr^{3+}, and Ce^{3+}. For the analysis, 50 nM concentrations of amino acids were incubated with CuO@DOP NPs (10 mM) for 10 min at room temperature, and further subjected to UV–vis absorption and fluorescence emission measurements.

The respective optimization of geometries, energy calculations and chemical interaction between the surface modifier and L-Cys moieties were properly described through DFT computations using conventional B3LYP method by employing 6-311G basis set [69]. All the computations were performed using GAUSSIAN 09 quantum mechanical package in assistance with GaussView version 5.0.

2.5. Estimation of L-Cys in blood and urine samples

The blood and urine samples were collected from the Government Medical College and Hospital (GMCH), Sector 32, Chandigarh, India. An appropriate volume of pre treated blood and urine samples were spiked with the different concentration of L-Cys (20–100 nM) for checking the usability of the prepared CuO@DOP NPs based bio sensor for the estimation of L-Cys in real samples.

3. Results and discussion

3.1. Structural and morphological characterization of CuO@DOP NPs

The synthesis of the surface functionalized CuO nanoparticles with DOP has been carried out by using the microwave assisted methodology. Fig. 2a has illustrated the formation of monoclinic geometry of CuO@DOP NPs with characteristic peaks at 31.75°, 35.89°, 39.17°, 44.05°, 52.56°, 59.13° and 62.5° respectively. The calculated average crystallite size is 10 nm. These peaks have been assigned to (110), (111), (111), (202), (020), (202) and (113) planes of CuO NPs [JCPDS (no-96-410-5686)] [70]. In addition, the absence of Cu(I) peak in the XRD spectra has further pointed out the formation of CuO NPs. The optical absorption and luminescence studies of CuO@DOP NPs have been investigated by using the UV–vis absorption and fluorescence spectroscopic analysis. Fig. 2b has shown the observable UV peak at 280 nm for synthesized CuO@DOP NPs. This peak has been mainly associated with the surface defects in the CuO NPs. UV–vis absorbance properties of CuO@DOP NPs as a function of concentration of $CuCl_2$ has been studied (Fig. S1 Supplementary data). The absorption peak was observed at 280 nm with the variation of concentration. In addition, the absorption value was found to enhance with increasing the concentration of copper salt up to 2.5 mM. After this concentration, there was a decrease in the absorption value for CuO@DOP NPs for 3.5 and 5 mM concentrations of copper salt. This decrease was mainly associated with the unavailability of reducing agents (dopamine 0.6 mM) for the complete reduction of $CuCl_2$ salt during the formation of CuO nanoparticles. Therefore, 2.5 mM concentration of $CuCl_2$ was optimized for the preparation of nanoparticles. The fluorescence emission spectra of CuO@DOP NPs has displayed a peak at 335 nm with λ_{exc} = 270 nm (Fig. 2b). FTIR analysis has been performed to understand the mode of attachment of dopamine over the surface of CuO NPs. Fig. 2c has displayed the FTIR spectra of pure DOP and CuO@DOP NPs. The characteristic peak of dopamine at 3340 and 3035 cm^{-1} has been assigned for active N—H primary amine stretching and —OH group moiety present on dopamine molecule [71]. The peak at 2936 and 2840 cm^{-1} has been aroused due to weak C—H stretching. The peak at 1618 cm^{-1} has been corresponded to the N—H bending [72]. The aromatic C=C stretching and C—O stretching peak has been profiled at 1485 and 1265 cm^{-1} respectively. Whereas the peak at 3014 cm^{-1} in CuO@DOP NPs has been aroused due to the adsorbed water molecules at the surface. The corresponding shift in peaks at 1620 (N—H bending), 1481(aromatic C=C stretching), 1263 (C—O stretching peak) in respect to pure dopamine has been associated with the electrostatic interactions between the DOP and CuO NPs. The sharp peak at 528 cm^{-1} has been assigned due to the Cu—O stretching [73] peak in CuO@DOP NPs. The thermal

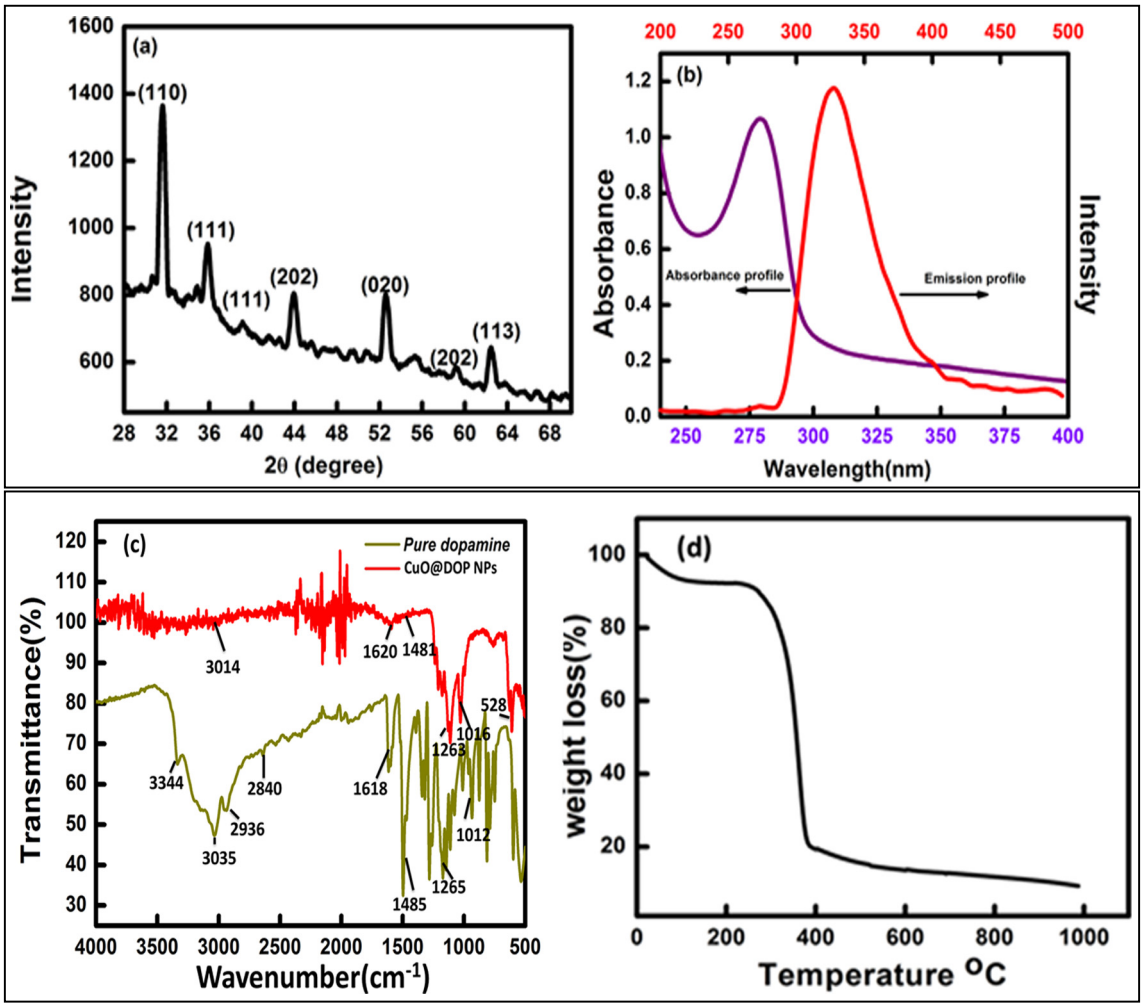

Fig. 2. (a) XRD spectra, (b) UV–vis with Fluorescence emission spectra (c) FTIR and (d) TGA spectral profile for CuO@DOP NPs.

decomposition properties of the CuO@DOP NPs have been analyzed by thermo gravimetric analysis (TGA). The result of TGA has directed the temperature-based mass loss curves for CuO@DOP NPs (Fig. 2d). The first major weight loss of 7.9% in the temperature range of 120–150 °C has been aroused due to the moisture loss from the sample [74]. The second major weight loss of 31.08% in the temperature range of 250–400 °C has been attributed to the decomposition of dopamine molecules [75] reacted with or physically adsorbed over the surface of CuO NPs. These respective changes have further supported the surface modification of CuO NPs with dopamine molecules.

HRTEM images have displayed the spherical morphology of CuO@DOP NPs (Fig. 3a) with average size ranging between 30 nm (Fig. 3b). The surface coating of DOP over CuO NPs has further been visualized by magnified HRTEM image of single CuO@DOP NPs (Fig. S2 Supplementary data). The uniform variation of contrast over the surface of CuO NPs has verified the templating effect of DOP over CuO NPs and controlled the rate of agglomeration during the synthesis of particles. The quantitative elemental analysis has been visualized by EDX data (Fig. 3c). The zeta potential value of as prepared nanoparticles has been found to be +7.86 mV (Fig. S3 Supplementary data). The presence of only Cu, O, C and N elements in the samples have confirmed the purity of the samples. The uniform coating of DOP has further been visualized in the FESEM images (Fig. 3d). The quantitative elemental mapping has further been carried out by using EDX studies. The presence of Cu, O, N and C has given an insight into the formation of CuO@DOP NPs (Fig. 3d).

The in vitro biocompatibility studies of CuO@DOP NPs have been studied as a function of concentration ranging between 1.56, 3.125, 6.25, and 12.5 μg/ml by using MTT assay for 24 h on mouse L929 fibroblastic cell lines. It has been found that the presence of CuO@DOP NPs has induced 70% viability of L929 normal cells up to 12.5 μg/ml (Fig. 4). The respective cell morphology and cell density has further been found to be intact in presence of CuO@DOP NPs. The prepared nanoparticles have the tendency to slow down the cell proliferation rather than killing them. Therefore, the results have confirmed the marginal in vitro biocompatibility of as prepared nanoparticles and required further in-depth studies for their future scope in medicine. The biocompatibility studies has also verified by testing the influence of CuO@DOP NPs on the growth of two bacterial strains viz. gram-positive (*Staphylococcus aureus*) and gram-negative (*Escherichia coli*) bacteria. The influence of concentration ranging 5 ppm, 10 ppm and 20 ppm of CuO@DOP NPs has been used for the analysis. The absence of zone of inhibition in both the chosen bacterial strains in all the employed concentrations has supported the non-toxic nature of CuO@DOP NPs.

3.2. Spectral response of the CuO@DOP NPs to L-Cys

In order to scrutinize the sensitivity of CuO@DOP NPs for the identification of L-Cys, we have carried out the optical absorbance and fluorescence emission behaviour of CuO@DOP NPs in presence of 15 different amino acids (Fig. 5a and b). For the optical analysis, 50 nM amount of respective amino acid has been prepared in solution of CuO@DOP NPs. From the spectra, it has been found that the optical

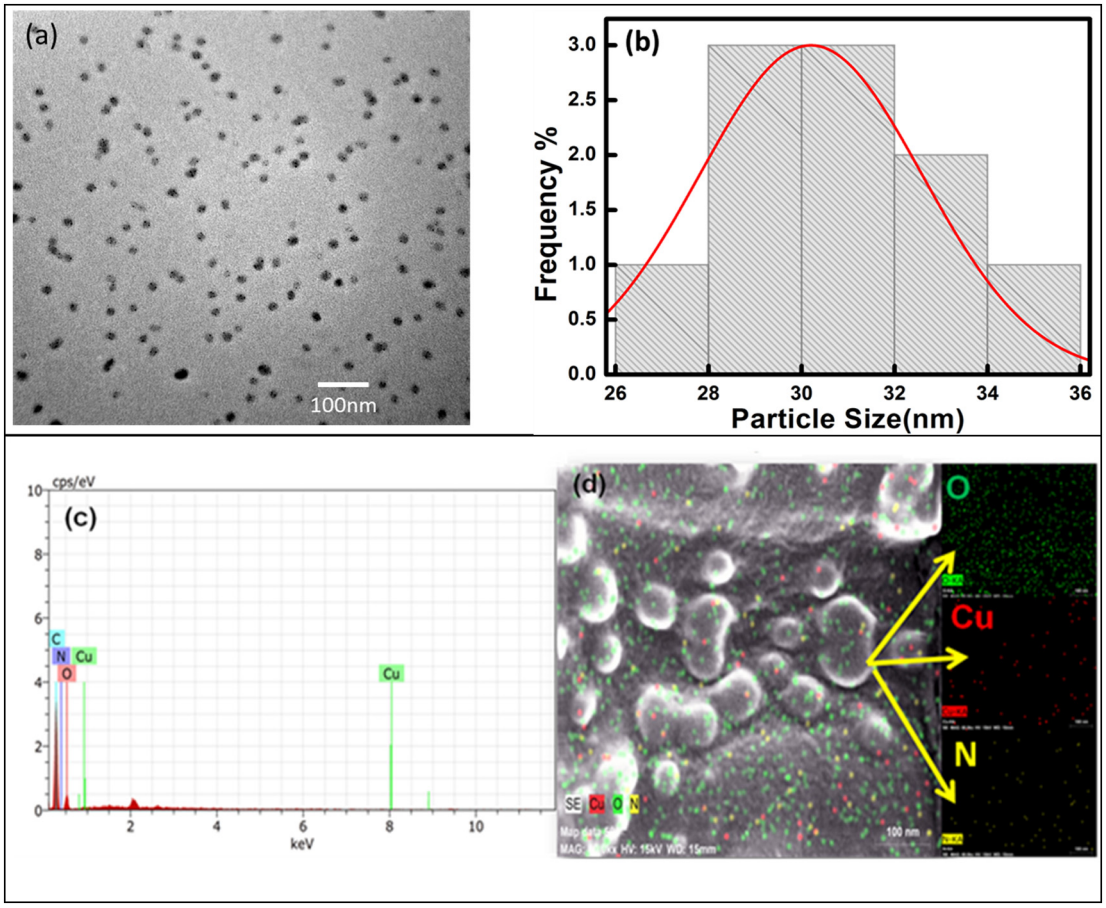

Fig. 3. (a) HRTEM, (b) histogram showing the size distribution, (c) EDX and (d) FESEM images with elemental mapping for CuO@DOP NPs.

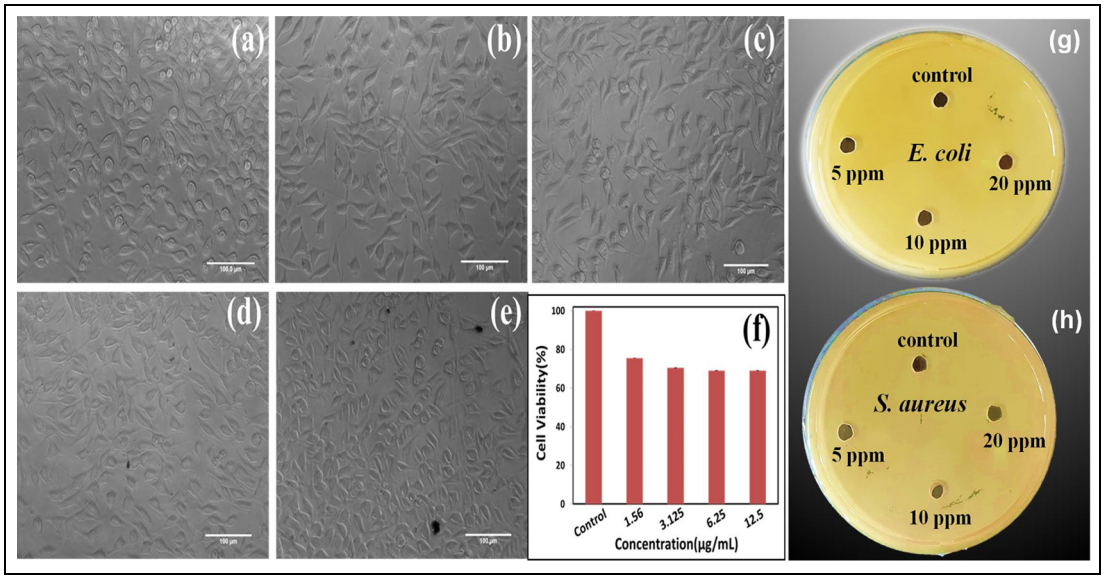

Fig. 4. Bright field images of mouse L929 fibroblastic cell line exposed to CuO@DOP NPs at concentrations (a) Control, (b) 1.56 μg/ml, (c) 3.125 μg/ml, (d) 6.25 μg/ml, (e) 12.5 μg/ml, (f) cell viability of L929 fibroblastic cell line. Antimicrobial activities of (g) *E. coli* and (h) *S. aureus* as function of concentration (5 ppm, 10 ppm and 20 ppm) of CuO@DOP NPs.

absorbance and emission intensity has shown enhancement in presence of L-Cys as compared to other chosen amino acids. In addition, the optical spectra have shown the blue shift in the peak position in presence of L-Cys (Fig. 5a). The solution has also displayed the visible colorimetric changes in presence of L-Cys (Fig. 5c).

The probable reason for the enhancement of absorbance and emission intensity has been explained on the basis of complexation and electrostatic interaction between CuO@DOP NPs and L-Cys molecules. It has been further associated with the increase in π-electron transfer to the vacant d orbital of metal ion, which has raised the energy of d-

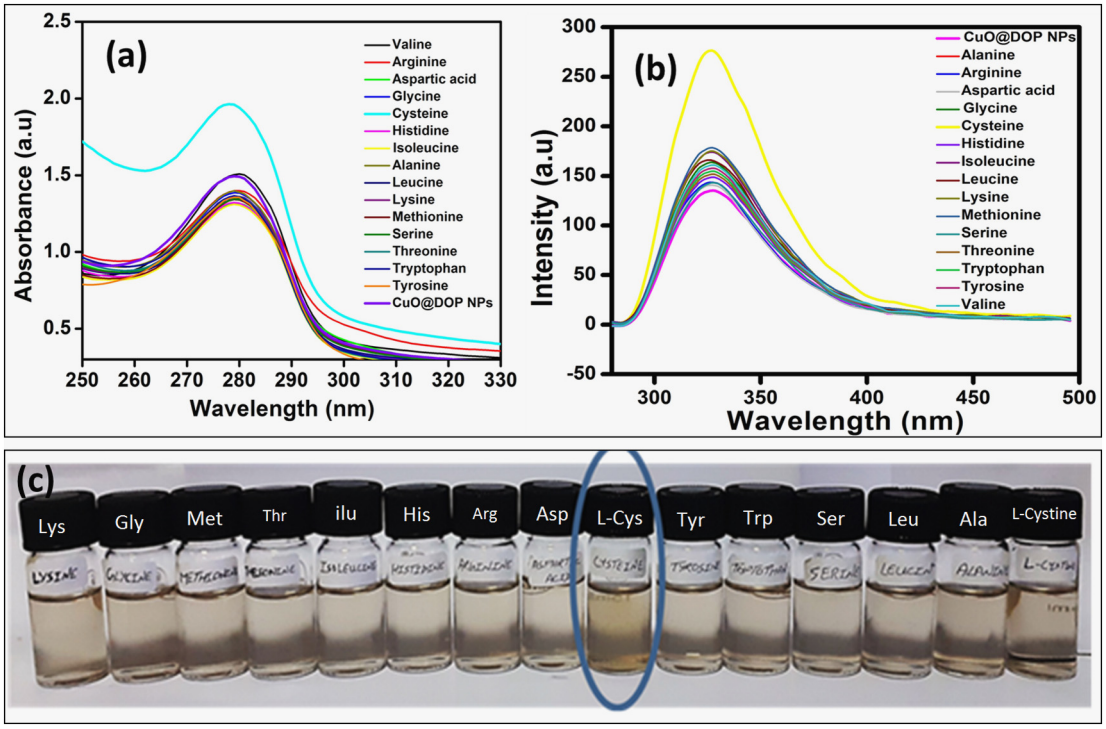

Fig. 5. (a) UV–vis absorbance, (b) fluorescence emission profile and (c) visual changes of CuO@DOP NPs in presence of different amino acids and showing their selectivity for L-Cys.

orbital and increased the intensity values. In comparison to other amino acids, the presence of sulphur in case of L-Cys has augmented the interaction between the CuO@DOP NPs and made the probe more selective for L-Cys as compared to other amino acids. The rapid sensitivity of the sensor towards L-Cys has further been tested by carrying out the time dependent absorption as well as fluorescence studies (Fig. S4 Supplementary data). The reproducibility of the CuO@DOP NPs in presence of L-cys has also been investigated to enhance the scope of the sensor (Fig. S5 Supplementary data). The digital photos as a function of response time in presence of L-Cys has also been presented to check the quick response time of the prepared CuO@DOP NPs based sensor for L-Cys.

The presence of the sulfhydryl group in L-Cys molecules have enhanced their scope of interaction with DOP capped CuO NPs [76]. The selectivity of as synthesized CuO@DOP NPs towards Cysteine among different thiolate group containing amino acids such as homocysteine and glutathione as well as in presence of Cystine and Met has also been checked. For the analysis, rate kinetic studies have been performed in presence of large excess of Cys, Hcy, or GSH (150 equiv.) over L-Cys (10 μM) in an aqueous solution at room temperature. The pseudo-first order kinetics has been followed by the samples (Fig. S5 Supplementary data) with rate constant values of 1.44×10^{-4}, 2.07×10^{-5}, 2.49×10^{-5}, 5.73×10^{-5} and 4.64×10^{-5} for L-Cys, cystine, GSH, Hcy and Met respectively. The higher value of rate constant for L-Cys among different thiolate group containing amino acids such as homocysteine and glutathione as well as in presence of Cystine and Met has supported the selectivity of sensor.

The interaction of CuO@DOP NPs has further been verified by using DFT computational studies by using conventional B3LYP method with 6-311G basis set. In general three attacking sites are available on DOP molecules for L-Cys (labelled as A, B, C in Fig. 6). The energy values for all these possible attacking sites of dopamine capped CuO NPs has been calculated in presence of L-Cys by using DFT studies (Fig. 6). Therefore, the prepared CuO@DOP NPs have used for distinguishing the molecules of L-Cys from other amino acids in physiological conditions. The respective values of Hartree energy (E_h) on attacking L-Cys on site A of CuO@DOP NPs has come out to be −2852.18 a.u as compared to −2851.13 a.u and −2850.21 a.u for site B and C respectively. Therefore, the most probable association of L-Cys is on site A of CuO@DOP NPs. The available attacking site and complexation via electron transfer process has enhanced the selectivity of CuO@DOP NPs towards L-Cys as compared to other amino acids.

In addition, the optical and fluorescence emission spectra of CuO@DOP NPs have further been investigated in presence of different concentrations of L-Cys ranging between 10 and 100 nM. Fig. 7a and b has shown the significant enhancement in the absorbance and fluorescence emission intensity as a function of concentration of L-Cys. There has been a good linear relationship between the absorbance values and fluorescence intensities of CuO@DOP NPs with regression coefficient values of 0.97 and 0.99 respectively (Fig. 7c and d).

The detection limit of L-Cys i.e. 35 nm has further been calculated by using LOD = 3 × standard deviation / slope (Fig. 7d). This higher value has supported the greater sensitivity of the sensor towards L-Cys. The obtained value has further been compared with the available sensors for L-cys. From the comparison it has been found that the prepared sensor has displayed higher limit of detection value (Table S1 Supplementary data). In order to study the selectivity of the prepared sensor, the fluorescence response of CuO@DOP NPs has been investigated in presence of series of interfering amino acid (150 μM) that may coexist with L-Cys (50 nM). From the data, it has been interpreted that in absence of L-Cys, the fluorescence response of CuO@DOP NPs has been decreased in presence of series of used interfering amino acid (Fig. 7e). However, the fluorescence response of CuO@DOP NPs has been significantly enhanced in presence of L-Cys and chosen interfering amino acid. The respective selectivity of our prepared sensor has also been verified in presence of series of metal ions (Fig. S6 Supplementary data). On interpreting the data, it has been found that in absence of L-Cys, the fluorescence response of CuO@DOP NPs has been decreased in presence of series of used metal ions (Fig. S6 Supplementary data). In addition, the fluorescence response of CuO@DOP NPs has been considerably boosted in existence of L-Cys and chosen interfering metal ions. The outcome has indicated the high selectivity of CuO@DOP NPs

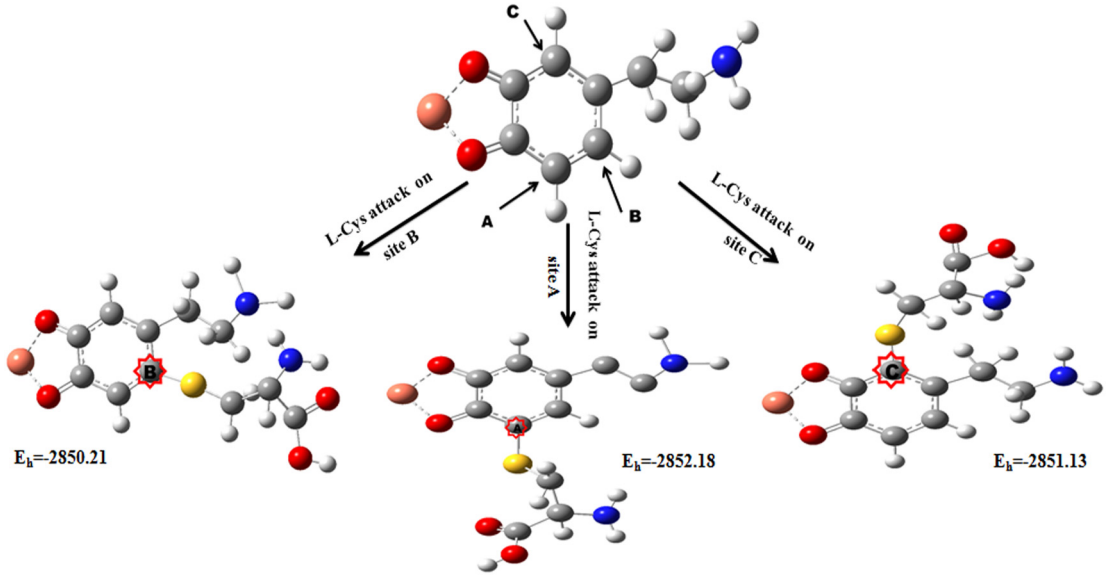

Fig. 6. 3D optimized molecular structure and their respective energy value calculation through DFT for CuO@DOP NPs in presence of L-Cys showing variable attacking sites (A, B, C) for L-Cys.

towards L-Cys and the coexisting interfering species has not affected the detection of L-Cys with CuO@DOP NPs. The corresponding UV–vis spectral and fluorescence changes of CuO@DOP NPs in presence of L-Cys has been tested via varying the pH of the reaction media. From the studies, it has been found that sensitivity was linearly dependent on the pH of the reaction media. The results have further supported the

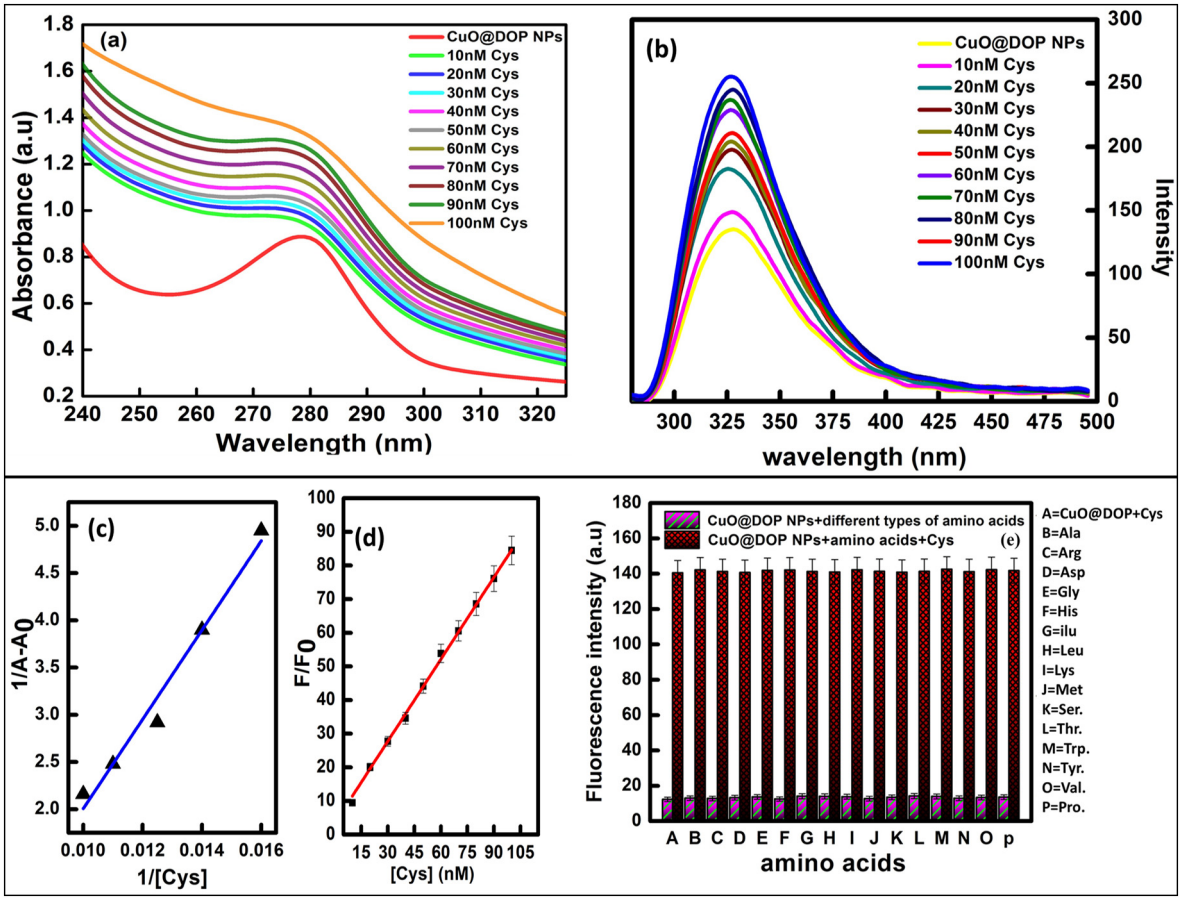

Fig. 7. (a) UV–vis absorption spectra and (b) fluorescence emission spectra of CuO@DOP NPs in the presence of increasing amounts of L-Cys, (c) Benesi–Hildebrand plot, and (d) Stern–Volmer plots for analyzing the interaction of CuO@DOP NPs with different concentrations of L-Cys. (e) Fluorescence responses of CuO@DOP NPs to various amino acids. The pink bars correspond to the emission changes of CuO@DOP NPs in the presence of different amino acids of interest. The green bars correspond to the changes of the emission that arises upon successive addition of L-Cys to the above solution. (For interpretation of the references to colour in this figure legend, the reader is referred to the web version of this article.)

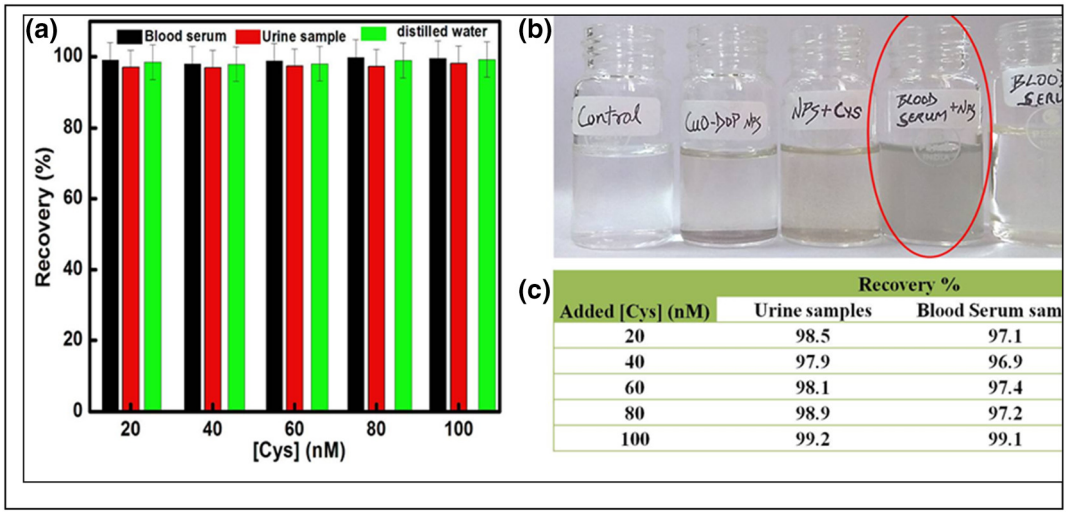

Added [Cys] (nM)	Recovery % Urine samples	Blood Serum sam
20	98.5	97.1
40	97.9	96.9
60	98.1	97.4
80	98.9	97.2
100	99.2	99.1

Fig. 8. (a, c) Recovery percentage studies and (b) colorimetric change of CuO@DOP NPs as a function of concentration of L-Cys in real samples of blood serum, urine and distilled water.

application of the prepared sensor for estimating L-Cys in blood and urine samples (Fig. S7 Supplementary data).

3.3. Estimation of L-Cys in blood and urine samples

In order to study the applicability of the prepared sensor in the biological samples, the utility of the prepared probe has been applied for estimating L-Cys in both blood serum and urine samples. The conventional addition technique has been used for the colorimetric analysis of L-Cys in blood serum (Fig. 8b) and urine samples (Fig. S8). For concise estimation, collected blood plasma and urine samples have been spiked with different concentration of L-Cys ranging from 10 to 100 nM (Fig. 8). For the measurements, the serum and urine samples have further been diluted to 100 times with buffer solution and centrifuged at 8000 rpm for 20 min. The obtained mixture has been incubated with CuO@DOP NPs for 10 min before taking the fluorescence emission profile for the samples. The fluorescence emission variations for each sample have been calculated from the linear calibration curve. Further recovery studies were also done to find percentage recovery. The result came for blood plasma and urine sample was shown in Fig. 8(a) and (b). In the case of a urine sample, the recovery percentage was comparable to 100% whereas for blood plasma, it was < 100% as compared to urine sample. The high values of recovery rate and visual changes of L-Cys in both blood plasma and urine samples have supported the high performance of the developed sensor towards L-Cys under physiological conditions.

4. Conclusion

In summary, we have designed a selective and sensitive fluorescence sensor of CuO@DOP NPs for the identification of L-Cys. The fabrication of the sensor has been achieved by using single step and cost effective microwave radiations based synthetic methodology. The biocompatible capping of dopamine have assisted the interaction of L-Cys and provided colorimetric and fluorescence response with detection limit of 0.35 nM. The interfering effect of other amino acids has also been studied to check the sensitivity and selectivity of the developed sensor. The practical application of designed sensor in human blood serum and urine sample has been tested towards colorimetric and fluorescence response. The high values of recovery rate (> 97%) of L-Cys in both blood serum and urine samples have supported the high performance of the developed sensor towards L-Cys under physiological conditions. A theoretical approach has been made to explore the interaction mechanism of CuO@DOP NPs with L-Cys by using DFT studies. Therefore, the current work has provided bio-compatible, cost effective, rapid and selective sensing of L-Cys in human blood and urine sample. The significant aspect of DOP@CuO has been associated with its biocompatibility and lower detection limit has assisted their pre-clinical applications and made it as a potential contender in bio-sensing applications.

Declaration of competing interest

The authors declare that they have no known competing financial interests or personal relationships that could have appeared to influence the work reported in this paper.

Acknowledgement

Savita Chaudhary is thankful for financial assistance provided by DST Purse grants II and DST Inspire Faculty award [IFACH-17] India. Deepak Rohilla is grateful to DST Haryana, India for JRF under Haryana State Council for Science and Technology fellowship scheme (HSCST/2533).

Appendix A. Supplementary data

Supplementary data to this article can be found online at https://doi.org/10.1016/j.msec.2020.110724.

References

[1] J. Yin, W. Ren, G. Yang, J. Duan, X. Huang, R. Fang, C. Li, T. Li, Y. Yin, Y. Hou, S.W. Kim, G. Wu, L-Cysteine metabolism and its nutritional implications, Mol. Nutr. Food Res. 60 (2016) 134–146, https://doi.org/10.1002/mnfr.201500031.
[2] C. Gotor, C. Álvarez, M.Á. Bermúdez, I. Moreno, I. García, L.C. Romero, Low abundance does not mean less importance in cysteine metabolism, Plant Signal. Behav. 5 (2010) 1028–1030, https://doi.org/10.4161/psb.5.8.12296.
[3] S.H. Lee, O.J. Sohn, Y.S. Yim, K.A. Han, G.W. Hyung, S.H. Chough, J. Il Rhee, Sequential injection analysis system for on-line monitoring of L-cysteine concentration in biological processes, Talanta 68 (2005) 187–192, https://doi.org/10.1016/j.talanta.2005.06.049.
[4] A.R. Frand, C.A. Kaiser, Two pairs of conserved cysteines are required for the oxidative activity of Ero1p in protein disulfide bond formation in the endoplasmic reticulum, Mol. Biol. Cell 11 (2000) 2833–2843, https://doi.org/10.1091/mbc.11.9.2833.
[5] S.E. Moriarty, J.H. Shah, M. Lynn, S. Jiang, K. Openo, D.P. Jones, P. Sternberg, Oxidation of glutathione and cysteine in human plasma associated with smoking, Free Radic. Biol. Med. 35 (2003) 1582–1588, https://doi.org/10.1016/j.freeradbiomed.2003.09.006.
[6] A. Falach-Malik, H. Rozenfeld, M. Chetboun, K. Rozenberg, U. Elyasiyan, S.R. Sampson, T. Rosenzweig, N-acetyl-L-cysteine inhibits the development of glucose intolerance and hepatic steatosis in diabetes-prone mice, Am. J. Transl. Res. 8 (2016) 3744–3756.

[7] W.W. Wang, S.Y. Qiao, D.F. Li, Amino acids and gut function, Amino Acids 37 (2009) 105–110, https://doi.org/10.1007/s00726-008-0152-4.

[8] N. Clemente Plaza, M. Reig García-Galbis, R.M. Martínez-Espinosa, Effects of the usage of L-cysteine (L-Cys) on human health, Molecules 23 (2018) 1–13, https://doi.org/10.3390/molecules23030575.

[9] Y. Luo, L. Zhang, W. Liu, Y. Yu, Y. Tian, A single biosensor for evaluating the levels of copper ion and L-cysteine in a live rat brain with alzheimer's disease, Angew. Chemie - Int. Ed. 54 (2015) 14053–14056, https://doi.org/10.1002/anie.201508635.

[10] L. Shao, H. Li, S.K. Pazhanisamy, A. Meng, Y. Wang, D. Zhou, Reactive oxygen species and hematopoietic stem cell senescence, Int. J. Hematol. 94 (2011) 24–32, https://doi.org/10.1007/s12185-011-0872-1.

[11] P.G. Paterson, A.W. Lyon, H. Kamencic, L.B. Andersen, B.H.J. Juurlink, Sulfur amino acid deficiency depresses brain glutathione concentration, Nutr. Neurosci. 4 (2001) 213–222, https://doi.org/10.1080/1028415X.2001.11747364.

[12] C. Bauchart-Thevret, B. Stoll, S. Chacko, D.G. Burrin, Sulfur amino acid deficiency upregulates intestinal methionine cycle activity and suppresses epithelial growth in neonatal pigs, Am. J. Physiol. Endocrinol. Metab. 296 (2009) 1239–1250, https://doi.org/10.1152/ajpendo.91021.2008.

[13] L. Hu, H. Cheng, Y. Gao, M. Shi, Y. Liu, Z. Hu, J. Xu, L. Qiu, W. Yuan, A.Y. Leung, Y. Yang, T. Cheng, Antioxidant N-acetyl-L-cysteine increases engraftment of human hematopoietic stem cells in immune-deficient mice, Blood 124 (2016) 45–49, https://doi.org/10.1182/blood-2014-03-559369.

[14] D.M. Townsend, K.D. Tew, H. Tapiero, The importance of glutathione in human disease, Biomed. Pharmacother. 57 (2003) 145–155, https://doi.org/10.1016/S0753-3322(03)00043-X.

[15] G. Chwatko, E. Bald, Determination of cysteine in human plasma by high-performance liquid chromatography and ultraviolet detection after pre-column derivatization with 2-chloro-1-methylpyridinium iodide, Talanta 52 (2000) 509–515, https://doi.org/10.1016/S0039-9140(00)00394-5.

[16] A. Küster, I. Tea, S. Sweeten, J.C. Rozé, R.J. Robins, D. Darmaun, Simultaneous determination of glutathione and cysteine concentrations and 2H enrichments in microvolumes of neonatal blood using gas chromatography-mass spectrometry, Anal. Bioanal. Chem. 390 (2008) 1403–1412, https://doi.org/10.1007/s00216-007-1799-5.

[17] J.M. Held, S.R. Danielson, J.B. Behring, C. Atsriku, D.J. Britton, R.L. Puckett, B. Schilling, J. Campisi, C.C. Benz, B.W. Gibson, Targeted quantitation of site-specific cysteine oxidation in endogenous proteins using a differential alkylation and multiple reaction monitoring mass spectrometry approach, Mol. Cell. Proteomics 9 (2010) 1400–1410, https://doi.org/10.1074/mcp.M900643-MCP200.

[18] C. Xiao, J. Chen, B. Liu, X. Chu, L. Wu, S. Yao, Sensitive and selective electrochemical sensing of L-cysteine based on a caterpillar-like manganese dioxide-carbon nanocomposite, Phys. Chem. Chem. Phys. 13 (2011) 1568–1574, https://doi.org/10.1039/c0cp00980f.

[19] M.L. Yola, V.K. Gupta, T. Eren, A.E. Şen, N. Atar, A novel electro analytical nanosensor based on graphene oxide/silver nanoparticles for simultaneous determination of quercetin and morin, Electrochim. Acta 120 (2014) 204–211, https://doi.org/10.1016/j.electacta.2013.12.086.

[20] F. Kardaş, M. Beytur, O. Akyıldırım, H. Yüksek, M.L. Yola, N. Atar, Electrochemical detection of atrazine in wastewater samples by copper oxide (CuO) nanoparticles ionic liquid modified electrode, J. Mol. Liq. 248 (2017) 360–363, https://doi.org/10.1016/j.molliq.2017. 10.085.

[21] R. Głowacki, E. Bald, Fully automated method for simultaneous determination of total cysteine, cysteinylglycine, glutathione and homocysteine in plasma by HPLC with UV absorbance detection, J. Chromatogr. B 877 (2009) 3400–3404, https://doi.org/10.1016/j.jchromb. 2009.06.012.

[22] Y.W. Wang, S. Tang, H.H. Yang, H. Song, A novel colorimetric assay for rapid detection of cysteine and Hg^{2+} based on gold clusters, Talanta 146 (2016) 71–74, https://doi.org/10.1016/j. talanta.2015.08.015.

[23] V.K. Gupta, N. Atar, M.L. Yola, Z. Üstündağ, L. Uzun, A novel magnetic Fe@Au core-shell nanoparticles anchored graphene oxide recyclable nanocatalyst for the reduction of nitrophenol compounds, Water Res. 48 (2014) 210–217, https://doi.org/10.1016/j.watres.2013.09. 027.

[24] S. Karthikeyan, V.K. Gupta, R. Boopathy, A. Titus, G. Sekaran, A new approach for the degradation of high concentration of aromatic amine by heterocatalytic Fenton oxidation: kinetic and spectroscopic studies, J. Mol. Liq. 173 (2012) 153–163, https://doi.org/10.1016/j.molliq. 2012.06.022.

[25] M.H. Dehghani, D. Sanaei, I. Ali, A. Bhatnagar, Removal of chromium(VI) from aqueous solution using treated waste newspaper as a low-cost adsorbent: kinetic modeling and isotherm studies, J. Mol. Liq. 215 (2016) 671–679, https://doi.org/10.1016/j.molliq.2015.12.057.

[26] A. Asfaram, M. Ghaedi, S. Agarwal, I. Tyagi, V.K. Gupta, Removal of basic dye Auramine-O by ZnS:Cu nanoparticles loaded on activated carbon: optimization of parameters using response surface methodology with central composite design, RSC Adv. 5 (2015) 18438–18450, https://doi.org/10.1039/c4ra15637d.

[27] V.K. Gupta, A.K. Singh, L.K. Kumawat, Thiazole Schiff base turn-on fluorescent chemosensor for Al^{3+} ion, Sensors Actuators B Chem. 195 (2014) 98–108, https://doi.org/10.1016/j. snb.2013.12.092.

[28] S.K. Srivastava, V.K. Gupta, S. Jain, PVC-based 2,2,2-cryptand sensor for zinc ions, Anal. Chem. 68 (1996) 1272–1275, https://doi.org/10.1021/ac9507000.

[29] V.K. Gupta, L.P. Singh, R. Singh, N. Upadhyay, S.P. Kaur, B. Sethi, A novel copper (II) selective sensor based on dimethyl 4,4′(o-phenylene) bis(3-thioallophanate) in PVC matrix, J. Mol. Liq. 174 (2012) 11–16, https://doi.org/10.1016/j.molliq.2012.07.016.

[30] V.K. Gupta, M. Al Khayat, A.K. Minocha, P. Kumar, Zinc(II)-selective sensors based on dibenzo-24-crown-8 in PVC matrix, Anal. Chim. Acta 532 (2005) 153–158, https://doi.org/10.1016/j.aca.2004.10.067.

[31] V.K. Gupta, N. Mergu, L.K. Kumawat, A.K. Singh, Selective naked-eye detection of magnesium (II) ions using a coumarin-derived fluorescent probe, Sensors Actuators B Chem. 207 ((2015) 216–223, https://doi.org/10.1016/j.snb.2014.10.044.

[32] H. Karimi-Maleh, F. Tahernejad-Javazmi, N. Atar, M.L. Yola, V.K. Gupta, A.A. Ensafi, A novel DNA biosensor based on a pencil graphite electrode modified with polypyrrole/functionalized multiwalled carbon nanotubes for determination of 6-mercaptopurine anticancer drug, Ind. Eng. Chem. Res. 54 (2015) 3634–3639, https://doi.org/10.1021/ie504438z.

[33] V. K. Gupta, A. Nayak, S. Agarwal, B. Singhal, Recent advances on potentiometric membrane sensors for pharmaceutical analysis, Comb. Chem. High Throughput Screen. 14 (2011) 284–302, https://doi.org/10.2174/138620711795222437.

[34] V.K. Gupta, B. Sethi, R.A. Sharma, S. Agarwal, A. Bharti, Mercury selective potentiometric sensor based on low rim functionalized thiacalix [4]-arene as a cationic receptor, J. Mol. Liq. 177 (2013) 114–118, https://doi.org/10.1016/j.molliq.2012.10.008.

[35] V.K. Gupta, S. Kumar, R. Singh, L.P. Singh, S.K. Shoora, B. Sethi, Cadmium (II) ion sensing through p-tert-butyl calix[6]arene based potentiometric sensor, J. Mol. Liq. 195 (2014) 65–68, https://doi.org/10.1016/j.molliq.2014.02.001.

[36] A.K. Jain, V.K. Gupta, L.P. Singh, Neutral carrier and organic resin based membranes as sensors for uranyl ions, Anal. Proc. Incl. Anal. Commun. 32 (1995) 263–266, https://doi.org/10.1039/AI9953200263.

[37] V.K. Gupta, M.R. Ganjali, P. Norouzi, H. Khani, A. Nayak, S. Agarwal, Electrochemical analysis of some toxic metals by ion-selective electrodes, Crit. Rev. Anal. Chem. 41 (2011) 282–313, https://doi.org/10.1080/10408347.2011.589773.

[38] S.K. Srivastava, V.K. Gupta, S. Jain, Determination of lead using a poly(vinyl chloride)-based crown ether membrane, Analyst 120 (1995) 495–498, https://doi.org/10.1039/an9952000495.

[39] S.K. Srivastava, V.K. Gupta, M.K. Dwivedi, S. Jain, Caesium PVC-crown (dibenzo-24-crown-8) based membrane sensor, Anal. Proc. Incl. Anal. Commun. 32 (1995) 21–23, https://doi.org/10.1039/AI9953200021.

[40] V.K. Gupta, H. Karimi-Maleh, R. Sadegh, Simultaneous determination of hydroxylamine, phenol and sulfite in water and waste water samples using a voltammetric nanosensor, Int. J. Electrochem. Sci. 10 (2015) 303–316.

[41] R.N. Goyal, V.K. Gupta, A. Sangal, N. Bachheti, Voltammetric determination of uric acid at a fullerene-C 60-modified glassy carbon electrode, Electroanalysis 17 (2005) 2217–2223, https://doi.org/10.1002/elan.200503353.

[42] X. Fu, J. Wen, J. Li, H. Lin, Y. Liu, X. Zhuang, C. Tian, L. Chen, Highly sensitive detection of prostate cancer specific PCA3 mimic DNA using SERS-based competitive lateral flow assay, Nanoscale 11 (2019) 15530–15536, https://doi.org/10.1039/c9nr04864b.

[43] X. Fu, Z. Cheng, J. Yu, P. Choo, L. Chen, J. Choo, A SERS-based lateral flow assay biosensor for highly sensitive detection of HIV-1 DNA, Biosens. Bioelectron. 78 (2016) 530–537, https://doi.org/10.1016/j.bios.2015.11.099.

[44] Z. Zhang, Z. Chen, F. Cheng, Y. Zhang, L. Chen, Highly sensitive on-site detection of glucose in human urine with naked eye based on enzymatic-like reaction mediated etching of gold nanorods, Biosens. Bioelectron. 89 (2017) 932–936, https://doi.org/10.1016/j.bios.2016.09. 090.

[45] Z. Zhang, H. Wang, Z. Chen, X. Wang, J. Choo, L. Chen, Plasmonic colorimetric sensors based on etching and growth of noble metal nanoparticles: strategies and applications, Biosens. Bioelectron. 114 (2018) 52–65, https://doi.org/10.1016/j.bios.2018.05.015.

[46] Z. Zhang, Z. Chen, S. Wang, F. Cheng, L. Chen, Iodine-mediated etching of gold nanorods for plasmonic ELISA based on colorimetric detection of alkaline phosphatase, ACS Appl. Mater. Interfaces 7 (2015) 27639–27645, https://doi.org/10.1021/acsami.5b07344.

[47] T. Lou, Z. Chen, Y. Wang, L. Chen, Blue-to-red colorimetric sensing strategy for Hg^{2+} and Ag^{+} via redox-regulated surface chemistry of gold nanoparticles, ACS Appl. Mater. Interfaces 3 (2011) 1568–1573, https://doi.org/10.1021/am200130e.

[48] X. Chen, Y. Zhou, X. Peng, J. Yoon, Fluorescent and colorimetric probes for detection of thiols, Chem. Soc. Rev. 39 (2010) 2120–2135, https://doi.org/10.1039/b925092a.

[49] X. Wang, J. Yu, J. Li, Q. Kang, D. Shen, L. Chen, Quantum dots based imprinting fluorescent nanosensor for the selective and sensitive detection of phycocyanin: a general imprinting strategy toward proteins, Sensors Actuators B Chem. 255 (2018) 268–274, https://doi.org/10.1016/j.snb.2017.08.068.

[50] X. Wang, J. Yu, X. Wu, J. Fu, Q. Kang, D. Shen, J. Li, L. Chen, A molecular imprinting-based turn-on Ratiometric fluorescence sensor for highly selective and sensitive detection of 2,4-dichlorophenoxyacetic acid (2,4-D), Biosens. Bioelectron. 81 (2016) 438–444, https://doi.org/10.1016/j.bios.2016.03.031.

[51] H. Zhang, N. Qin, Z. Fang, A novel dicyanoisophorone-based ratiometric fluorescent probe for selective detection of cysteine and its bioimaging application in living cells, Molecules 23 (2018) 1–9, https://doi.org/10.3390/molecules23020475.

[52] Y.H. Zhao, Y. Luo, H. Wang, T. Guo, H. Zhou, H. Tan, Z. Zhou, Y. Long, Z. Tang, A new fluorescent probe based on aggregation induced emission for selective and quantitative determination of copper(II) and its further application to cysteine detection, ChemistrySelect 3 (2018) 1521–1526, https://doi.org/10.1002/slct.201702603.

[53] S. Manna, P. Karmakar, S.S. Ali, U.N. Guria, S.K. Samanta, R. Sarkar, P. Datta, A.K. Mahapatra, A highly selective ICT-based fluorescent probe for cysteine sensing and its application in living cell imaging, Anal. Methods 11 (2019) 1192–1198, https://doi.org/10.1039/c8ay02651c.

[54] Y.S. Yang, Z.H. Yuan, X.P. Zhang, J.F. Xu, P.C. Lv, H.L. Zhu, A selective fluorescent sensor for cysteine detection with potential as a white light emitting fluorophore in living cell imaging, J. Mater. Chem. B 7 (2019) 2911–2914, https://doi.org/10.

1039/c9tb00273a.
[55] Y. Wang, Q. Meng, Q. Han, G. He, Y. Hu, H. Feng, H. Jia, R. Zhang, Z. Zhang, Selective and sensitive detection of cysteine in water and live cells using a coumarin-Cu^{2+} fluorescent ensemble, New J. Chem. 42 (2018) 15839–15846, https://doi.org/10.1039/c8nj03809k.
[56] L. Zhang, Q.Y. Cai, J. Li, J. Ge, J.Y. Wang, Z.Z. Dong, Z.H. Li, A label-free method for detecting biothiols based on poly(thymine)-templated copper nanoparticles, Biosens. Bioelectron. 69 (2015) 77–82, https://doi.org/10.1016/j.bios.2015.02.012.
[57] X. Fu, L. Chen, J. Li, M. Lin, H. You, W. Wang, Label-free colorimetric sensor for ultrasensitive detection of heparin based on color quenching of gold nanorods by graphene oxide, Biosens. Bioelectron. 34 (2012) 227–231, https://doi.org/10.1016/j.bios.2012.02.008.
[58] J. Ge, Z. Qi, L. Zhang, A simple and sensitive fluorescence assay for biothiol and acetylcholinesterase activity detection based on a HSA-AuNCs@Cu^{2+} complex, Anal. Methods 11 (2019) 5031–5037, https://doi.org/10.1039/c9ay01815h.
[59] Z. Huang, C. Wu, Y. Li, Z. Zhou, R. Xie, X. Pang, H. Xu, H. Li, Y. Zhang, A fluorescent probe for the specific detection of cysteine in human serum samples, Anal. Methods 11 (2019) 3280–3285, https://doi.org/10.1039/c9ay00659a.
[60] A. Mokhtari, A. Goudarzi, M. Benam, S. Mehdizadeh Langroodi, S. Karimmohammad, M. Keyvanfard, Fabrication and characterization of $Cu(OH)_2$/CuO nanowires as a novel sensitivity enhancer of the luminol-H_2O_2 chemiluminescence system: determination of cysteine in human plasma, RSC Adv. 6 (2016) 5320–5329, https://doi.org/10.1039/c5ra21085b.
[61] H. Liu, Y. Sun, J. Yang, Y. Hu, R. Yang, Z. Li, L. Qu, Y. Lin, High performance fluorescence biosensing of cysteine in human serum with superior specificity based on carbon dots and cobalt-derived recognition, Sensors Actuators B Chem. 280 (2019) 62–68, https://doi.org/10.1016/j.snb.2018.10. 029.
[62] V.K. Gupta, N. Mergu, L.K. Kumawat, A.K. Singh, A reversible fluorescence "off-on-off" sensor for sequential detection of aluminum and acetate/fluoride ions, Talanta 144 (2015) 80–89, https://doi.org/10.1016/j.talanta.2015.05.053.
[63] F. Kardaş, M. Beytur, O. Akyıldırım, H. Yüksek, M.L. Yola, N. Atar, Electrochemical detection of atrazine in wastewater samples by copper oxide (CuO) nanoparticles ionic liquid modified electrode, J. Mol. Liq. 248 (2017) 360–363, https://doi.org/10.1016/j. molliq.2017. 10.085.
[64] I. Analytical, copper(Il)-selective electrodes based on macrocyclic compounds, A. Proceedings 32 (1995) 99–101.
[65] M.D. Shultz, J.U. Reveles, S.N. Khanna, E.E. Carpenter, Reactive nature of dopamine as a surface functionalization agent in iron oxide nanoparticles, J. Am. Chem. Soc. 129 (2007) 2482–2487, https://doi.org/10.1021/ja0651963.
[66] Z. Shan Hong, Y. Cao, J. fa Deng, A convenient alcohothermal approach for low temperature synthesis of CuO nanoparticles, Mater. Lett. 52 (2002) 34–38, https://doi.org/10.1016/S0167-577X(01)00361-5.
[67] T. Espevik, J. Nissen-Meyer, A highly sensitive cell line, WEHI 164 clone 13, for measuring cytotoxic factor/tumor necrosis factor from human monocytes, J. Immunol. Methods 95 (1986) 99–105, https://doi.org/10.1016/0022-1759(86)90322-4.
[68] S. Chaudhary, D. Rohilla, A. Umar, N. Kaur, A. Shanavas, Synthesis and characterizations of luminescent copper oxide nanoparticles: toxicological profiling and sensing applications, Ceram. Int. 45 (2019) 15025–15035, https://doi.org/10.1016/j. ceramint. 2019. 04.239.
[69] X. Xu, W.A. Goddard, The X3LYP extended density functional for accurate descriptions of nonbond interactions, spin states, and thermochemical properties, Proc. Natl. Acad. Sci. U. S. A. 101 (2004) 2673–2677, https://doi.org/10.1073/pnas.0308730100.
[70] S.B. Maddinedi, B.K. Mandal, Peroxidase like activity of quinic acid stabilized copper oxide nanosheets, J. Anal. Pharm. Chem. 1 (2014) 1008–1011.
[71] B. Geiseler, M. Miljevic, P. Müller, L. Fruk, Phototriggered production of reactive oxygen species by TiO_2 nanospheres and rods, J. Nanomater. 2012 (2012) 1–9, https://doi.org/10.1155/2012/708519.
[72] P.J. Thistlethwaite, M.S. Hook, Diffuse reflectance Fourier transform infrared study of the adsorption of oleate/oleic acid onto titania, Langmuir 16 (2000) 4993–4998, https://doi.org/10.1021/la991514i.
[73] A.S. Ethiraj, D.J. Kang, Synthesis and characterization of CuO nanowires by a simple wet chemical method, Nanoscale Res. Lett. 7 (2012) 1–12, https://doi.org/10.1186/1556-276X-7-70.
[74] E. Delahaye, R. Göbel, R. Löbbicke, R. Guillot, C. Sieber, A. Taubert, Silica ionogels for proton transport, J. Mater. Chem. 22 (2012) 17140–17146, https://doi.org/10.1039/c2jm00037g.
[75] G. Liu, T. Zhou, W. Liu, S. Hu, F. Pan, H. Wu, Z. Jiang, B. Wang, J. Yang, X. Cao, Enhanced desulfurization performance of PDMS membranes by incorporating silver decorated dopamine nanoparticles, J. Mater. Chem. A 2 (2014) 12907–12917, https://doi.org/10.1039/c4ta01778a.
[76] R.E. Whitehead, J.V. Ferrer, J.A. Javitch, J.B. Justice, Reaction of oxidized dopamine with endogenous cysteine residues in the human dopamine transporter, J. Neurochem. 76 (2001) 1242–1251, https://doi.org/10.1046/j.1471-4159.2001.00125.x.